The ALMA REBELS survey: the cosmic H I gas mass density in galaxies at z = 7

Heintz, K.E.; Oesch, P.A.; Aravena, M.; Bouwens, R.J.; Dayal, P.; Ferrara, A.; ... ; Werf, P.P. van der

Note: To cite this publication please use the final published version (if applicable).

The ALMA REBELS Survey: The Cosmic H I Gas Mass Density in Galaxies at $z \approx 7$

K. E. Heintz[1,2] , P. A. Oesch[1,2,3] , M. Aravena[4] , R. J. Bouwens[5] , P. Dayal[6] , A. Ferrara[7] , Y. Fudamoto[8,9] ,
L. Graziani[10,11] , H. Inami[12] , L. Sommovigo[7] , R. Smit[13] , M. Stefanon[14] , M. Topping[15] , A. Pallottini[7] , and
P. van der Werf[5]

[1] Cosmic Dawn Center (DAWN), Denmark; keheintz@nbi.ku.dk
[2] Niels Bohr Institute, University of Copenhagen, Jagtvej 128, DK-2200 Copenhagen N, Denmark
[3] University of Geneva, Department of Astronomy, Chemin Pegasi 51, 1290 Versoix, Switzerland
[4] Nucleo de Astronomia, Facultad de Ingenieria y Ciencias, Universidad Diego Portales, Av. Ejercito 441, Santiago, Chile
[5] Leiden Observatory, Leiden University, NL-2300 RA Leiden, The Netherlands
[6] Kapteyn Astronomical Institute, University of Groningen, P.O. Box 800, 9700 AV Groningen, The Netherlands
[7] Scuola Normale Superiore, Piazza dei Cavalieri 7, I-56126 Pisa, Italy
[8] Waseda Research Institute for Science and Engineering, Faculty of Science and Engineering, Waseda University, 3-4-1 Okubo, Shinjuku, Tokyo 169-8555, Japan
[9] National Astronomical Observatory of Japan, 2-21-1, Osawa, Mitaka, Tokyo, Japan
[10] Dipartimento di Fisica, Sapienza, Università di Roma, Piazzale Aldo Moro 5, I-00185 Roma, Italy
[11] INAF/Osservatorio Astronomico di Roma, via Frascati 33, I-00078 Monte Porzio Catone, Roma, Italy
[12] Hiroshima Astrophysical Science Center, Hiroshima University, 1-3-1 Kagamiyama, Higashi-Hiroshima, Hiroshima 739-8526, Japan
[13] Astrophysics Research Institute, Liverpool John Moores University, 146 Brownlow Hill, Liverpool L3 5RF, UK
[14] Departament d'Astronomia i Astrofísica, Universitat de València, C. Dr. Moliner 50, E-46100 Burjassot, València, Spain
[15] Steward Observatory, University of Arizona, 933 N Cherry Avenue, Tucson, AZ 85721, USA

Abstract

The neutral atomic gas content of individual galaxies at large cosmological distances has until recently been difficult to measure due to the weakness of the hyperfine H I 21 cm transition. Here we estimate the H I gas mass of a sample of main-sequence star-forming galaxies at $z \sim 6.5$–7.8 surveyed for [C II] 158 μm emission as part of the Reionization Era Bright Emission Line Survey (REBELS), using a recent calibration of the [C II]-to-H I conversion factor. We find that the H I gas mass excess in galaxies increases as a function of redshift, with an average of $M_{HI}/M_\star \approx 10$, corresponding to H I gas mass fractions of $f_{HI} = M_{HI}/(M_\star + M_{HI}) = 90\%$, at $z \approx 7$. Based on the [C II] 158 μm luminosity function (LF) derived from the same sample of galaxies, we further place constraints on the cosmic H I gas mass density in galaxies (ρ_{HI}) at this redshift, which we measure to be $\rho_{HI} = 7.1^{+6.4}_{-3.0} \times 10^6 \, M_\odot \, \mathrm{Mpc}^{-3}$. This estimate is substantially lower by a factor of ≈ 10 than that inferred from an extrapolation of damped Lyα absorber (DLA) measurements and largely depends on the exact [C II] LF adopted. However, we find this decrease in ρ_{HI} to be consistent with recent simulations and argue that this apparent discrepancy is likely a consequence of the DLA sight lines predominantly probing the substantial fraction of H I gas in high-z galactic halos, whereas [C II] traces the H I in the ISM associated with star formation. We make predictions for this buildup of neutral gas in galaxies as a function of redshift, showing that at $z \gtrsim 5$, only $\approx 10\%$ of the cosmic H I gas content is confined in galaxies and associated with the star-forming ISM.

Unified Astronomy Thesaurus concepts: High-redshift galaxies (734); Galaxy evolution (594); Interstellar medium (847)

1. Introduction

In the modern cosmological framework, the first epoch of galaxy formation and reionization is initiated by the infall of neutral, pristine gas (Dayal & Ferrara 2018). Through the hierarchical formation of structure, the accretion and gravitational collapse of a significant fraction of this gas allow it to condense into gaseous "protogalactic" halos. This gas can internally cool and form dense molecular clouds that will eventually ignite and start producing stars. The neutral atomic hydrogen (H I) gas content is therefore a fundamental component in the formation and evolution of the first generation of galaxies.

In the local universe, the H I gas component in galaxies can be directly measured via the hyperfine H I 21 cm line emission (Zwaan et al. 2005; Walter et al. 2008; Leroy et al. 2008).

However, due to the weakness of the line, this feature can only be detected for individual galaxies out to modest cosmological distances (the most distant being located at $z = 0.367$; Fernández et al. 2016). Recent advances measuring the integrated 21 cm signal from thousands of galaxies have pushed this technique out to $z \approx 1$, providing a census of the average H I gas content of star-forming galaxies at this redshift (Chowdhury et al. 2020, 2021).

Alternatively, H I can be detected in absorption via the 21 cm or damped Lyα absorption (DLA) features imprinted from foreground galaxies toward bright background quasars (Péroux et al. 2003). This has enabled independent measurements of the cosmic H I gas mass density from $z \sim 0$–5 (Prochaska & Wolfe 2009; Noterdaeme et al. 2012; Neeleman et al. 2016). However, there are some uncertainties in how these DLA systems trace the star-forming galaxy population, with recent results showing that they predominantly probe the extended H I in the halos of galaxies (Neeleman et al. 2019). These extended H I gas reservoirs therefore do not represent the neutral gas associated with star formation. Further, this approach of

measuring H I is naturally limited to $z \lesssim 5$ due to the onset of the Lyα forest and the increasing Gunn–Peterson effect, significantly hindering measurements of DLA features in intervening galaxies at these early epochs (but see, e.g., Bañados et al. 2019).

Due to these limitations, the most promising approach to obtain a census of the overall H I gas content of galaxies beyond $z \gtrsim 5$ may be to use a suitable tracer of this cold neutral gas phase. Similar approaches based on the emission from carbon monoxide (CO; Tacconi et al. 2010, 2018), neutral atomic carbon (C I; Papadopoulos et al. 2004; Walter et al. 2011; Valentino et al. 2018), or dust (Magdis et al. 2012; Scoville et al. 2017) are commonly used to infer the molecular gas mass of galaxies through their connection to molecular hydrogen, H_2 (Bolatto et al. 2013). Similarly, it is of great interest to establish a feasible, alternative proxy for H I.

The bright infrared fine-structure transition of ionized carbon [C II] 158 μm is a promising tracer of gas in the most distant galaxies (Carilli & Walter 2013), even reaching into the epoch of reionization at $z \gtrsim 6$ (e.g., Smit et al. 2018; Hashimoto et al. 2019; Matthee et al. 2019; Schouws et al. 2022). The relatively low ionization potential of C (IP = 11.26 eV) causes a significant fraction of carbon in the neutral gas phase to be ionized to C^+ due to the permeating interstellar radiation field. [C II] emission has indeed been observed to originate partly from the neutral gas phase in the Milky Way and nearby galaxies (e.g., Madden et al. 1993, 1997; Pineda et al. 2014; Croxall et al. 2017), with growing evidence in high-redshift galaxies as well (e.g., Novak et al. 2019; Meyer et al. 2022). However, some contributions to the total emission are also expected from the ionized gas and molecular regions (e.g., Olsen et al. 2015; Vallini et al. 2017; Pallottini et al. 2019), though simulations of galaxies at $z \approx 6$ predict [C II] to predominantly originate from the neutral ISM (Katz et al. 2017; Ramos Padilla et al. 2022). In a recent study, Heintz et al. (2021) determined an empirical relation, specifically linking the [C II] 158 μm line emission to the total H I gas mass in galaxies. This [C II]-to-H I conversion factor (here denoted $\beta_{[CII]}$) appears universal in galaxies from $z \sim 6.5$ to $z \sim 0$, based on simulations and direct observations.

Here we apply this $\beta_{[CII]}$ conversion factor to infer the H I gas content of a statistical sample of UV-selected star-forming galaxies at $z \sim 6.5$–7.8, surveyed for [C II] 158 μm emission as part of the Reionization Era Bright Emission Line Survey (REBELS; Bouwens et al. 2022). The molecular gas content of these galaxies will be studied in a separate work (M. Aravena et al. 2022, in preparation). The stellar masses and star formation rates (SFRs) of these galaxies are representative of the high-mass end of the main sequence at this epoch (e.g., Topping et al. 2022). In Section 2 we introduce the sample and describe the methodology. In Section 3 we present our results. In Section 4 we discuss the implications of the inferred global H I gas content for the evolution of galaxies in the reionization epoch and we conclude on our work in Section 5.

Throughout the paper, we assume the concordance ΛCDM cosmological model with $\Omega_m = 0.315$, $\Omega_\Lambda = 0.685$, and $H_0 = 67.4 \, \mathrm{km \, s^{-1} \, Mpc^{-1}}$ (Planck Collaboration et al. 2020) and adopt a Chabrier (2003) initial mass function (IMF).

2. Sample and Methodology

REBELS targeted 40 galaxies at $z \sim 6.5$–9.0 selected from fields with deep photometric auxiliary data, as presented in

Bouwens et al. (2022). We adopt the total SFRs (UV + IR) and stellar masses presented by Topping et al. (2022) here. They are in the range $M_\star = 6.5 \times 10^8$–$3.1 \times 10^{10} M_\odot$ and SFRs = 10–200 $M_\odot \, \mathrm{yr^{-1}}$, determined by modeling the spectral energy distribution (SED) for each source with Prospector (Leja et al. 2017) assuming a nonparametric star formation history. The inferred stellar masses are generally higher than those for models assuming a constant star formation history. Of the surveyed galaxies, 23 were detected in [C II], with luminosities ranging from $L_{[CII]} = 1.3 \times 10^8 L_\odot$ to $1.7 \times 10^9 L_\odot$ (S. Schouws et al. 2022, in preparation). Other recent results from the REBELS survey include constraints on the dust properties, masses and temperatures (Dayal et al. 2022; Ferrara et al. 2022; Inami et al. 2022; Sommovigo et al. 2022), sizes and morphologies of the [C II] emission components (Fudamoto et al. 2022), and the efficiency of Lyα transmission (Endsley et al. 2022) of galaxies during the epoch of reionization.

To apply the metallicity-dependent [C II]-to-H I conversion factor derived by Heintz et al. (2021), we first need to infer the gas-phase metallicity for each galaxy in the sample. We adopt the fundamental $M_\star$-SFR-metallicity relation from Curti et al. (2020), parameterized as

$$Z(M_\star, \mathrm{SFR}) = Z_0 - \gamma/\beta \log(1 + (M_\star/M_0(\mathrm{SFR}))^{-\beta}) \quad (1)$$

where $M_0(\mathrm{SFR}) = 10^{m_0} \times \mathrm{SFR}^{m_1}$. We adopt their best-fitting parameters considering the total SFR: $Z_0 = 8.779$, $m_0 = 10.11$, $m_1 = 0.56$, $\gamma = 0.31$, and $\beta = 2.1$. This yields a range in metallicities for the REBELS sample of $12 + \log(\mathrm{O/H}) = 8.0 - 8.6$ ($\log Z/Z_\odot = -0.7$ to -0.1), with a mean and median value of 8.40 and 8.39, respectively. We caution, however, that this fundamental plane relation is not well established at $z \gtrsim 3$. These estimates should therefore only be taken as indicative of the actual metallicities. The recent calibrations provided by the Astraeus simulation framework (Hutter et al. 2021; Ucci et al. 2021) indeed seem to indicate overall lower metallicities at the same SFRs and stellar masses, but to be conservative, we adopt the empirical relation from Curti et al. (2020), effectively providing a lower bound on M_{HI}. Our metallicity estimates are also in good agreement with measurements of individual star-forming galaxies at similar redshifts (Jones et al. 2020) and follow the expected decrease in metallicity as a function of redshift (Sanders et al. 2021).

Based on the inferred gas-phase metallicity and the measured $L_{[CII]}$ for each galaxy, we estimate the H I gas mass using the $\beta_{[CII]}$ conversion factor

$$\log \beta_{[CII]} = \log M_{HI}/L_{[CII]} = (-0.87 \pm 0.09)$$
$$\times \log(Z/Z_\odot) + (1.48 \pm 0.12) \quad (2)$$

calibrated by Heintz et al. (2021), where $Z/Z_\odot$ is the relative solar abundance with $12 + \log(\mathrm{O/H})_\odot = 8.69$ for $\log(Z/Z_\odot) = 0$ (Asplund et al. 2009), and M_{HI} and $L_{[CII]}$ are in units of $M_\odot$ and $L_\odot$, respectively. This calibration is measured directly in galaxies at $z \sim 2$–6 through pencil-beam sight lines from γ-ray burst (GRB) afterglows and absorption-line spectroscopy. This approach does not assume or require that [C II] and H I have to be physically associated, though this seems to be evident from the absorption-line spectra. The derived $\beta_{[CII]}$ abundance ratio simply provides a measure of the total "column" [C II] luminosity, irrespective of the phase
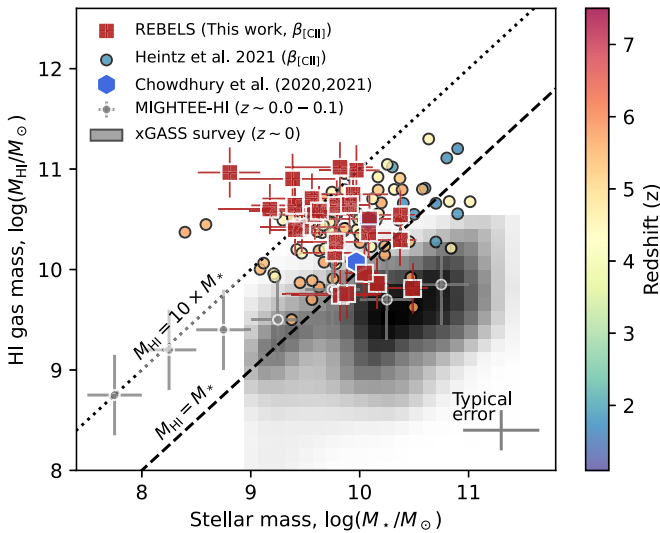
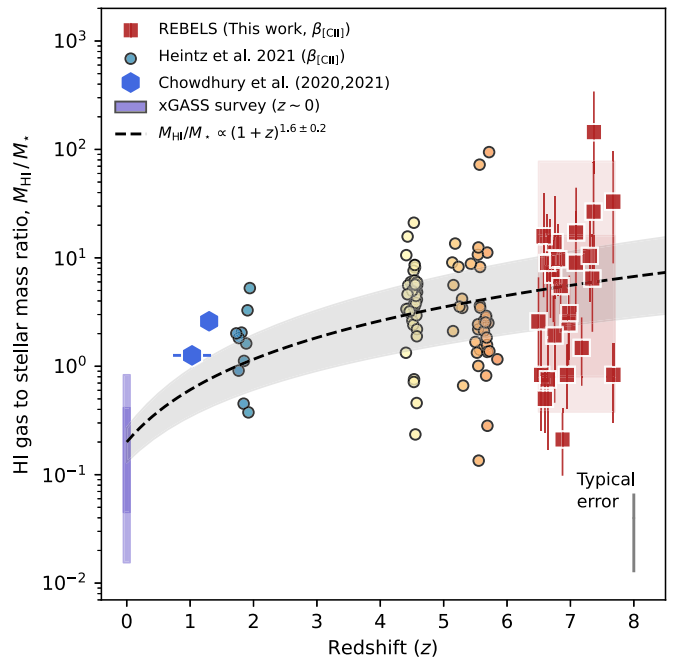**Figure 1.** H I gas and stellar-mass distributions of the REBELS sample galaxies at $z \sim 6.5$–7.8 (red squares). The inferred H I gas and stellar masses based on the $\beta_{[CII]}$ calibration of other high-redshift galaxy samples, color-coded as a function of redshift, are shown for comparison (see text and Heintz et al. 2021 for references), in addition to the average H I gas mass excess inferred by Chowdhury et al. (2020, 2021) from a stack of the 21 cm signal from galaxies at $z \approx 1$–1.3 (blue hexagons). The uncertainties on the REBELS sources are marked individually, and typical uncertainties for the other samples relying on $\beta_{[CII]}$ are shown as well. The xGASS sample represents galaxies at $z \sim 0$ with direct 21 cm H I observations. Diagonal lines mark $M_{HI}/M_\star = 1$–10.

Figure 2. Redshift evolution of $M_{HI}/M_\star$. The symbol notation follows Figure 1. The uncertainties on the REBELS sources (red squares) are marked individually, and typical uncertainties for the other samples relying on $\beta_{[CII]}$ are shown as well. The red- and purple-colored boxes mark vertically the 68% and 95% distributions of the REBELS and xGASS samples, respectively, and horizontally span the full redshift distribution. The average $M_{HI}/M_\star$ ratio is observed to gradually increase from $z \sim 0$ to $z \sim 7$, following approximately $M_{HI}/M_\star \propto (1 + z)^{1.6 \pm 0.2}$ (black dashed line).

it originates from, and relates it to the H I column density in the same sight line. This ratio is, however, assumed to be representative of the galaxy average. A similar methodology was used to derive an accurate [C I]-to-H_2 conversion factor in equivalent high-z absorption-selected galaxies (Heintz & Watson 2020). The $\beta_{[CII]}$ calibration was further supported and observed to show remarkable consistency with local dwarf galaxies at $z \sim 0$ from the Herschel Dwarf Galaxy Survey (Madden et al. 2013), for which [C II] luminosities and H I gas masses have been measured from direct 21 cm observations (Rémy-Ruyer et al. 2014; Cormier et al. 2015) and simulations of galaxies at similar redshifts. The metallicity-dependent [C II]-to-H I $\beta_{[CII]}$ conversion factor thus appears to be universal across redshifts. With a systematic uncertainty of 0.3 dex on the inferred metallicities, an additional 0.25 dex uncertainty will be propagated to $\log M_{HI}$ following this relation, which we assume throughout. We also note that if the actual metallicities are potentially underestimated as described above, the estimates of M_{HI} should effectively be treated as lower limits. The observed anticorrelation with metallicity of the $\beta_{[CII]}$ conversion factor is primarily a consequence of the increasing C/H abundance with increasing gas-phase metallicity.

3. Results

We derive H I gas masses in the range $M_{HI} = 5.5 \times 10^9 M_\odot$ to $1.0 \times 10^{11} M_\odot$ for the REBELS galaxy sample at $z \sim 6.5$–7.8. We find $M_{HI} > M_\star$ for the majority of systems, with mean and median values of $M_{HI}/M_\star = 13.3$ and 6.4, respectively, corresponding to H I gas mass fractions of $f_{HI} = M_{HI}/(M_\star + M_{HI}) = 86\%$ and 93%. These estimates are

in excellent agreement with the gas fractions of galaxies at $z \gtrsim 6$ predicted by the Astraeus simulations (Ucci et al. 2021). The M_{HI} versus $M_\star$ distributions are presented in Figure 1. For comparison, we overplot as 2D density contours in the M_{HI}–$M_\star$ parameter space the extended GALEX Arecibo SDSS Survey (xGASS) catalog of galaxies at $z \sim 0$ with direct H I 21 cm observations (Catinella et al. 2018). We also include the median measurements of the Early Science galaxies from the MIGHTEE H I emission project covering $z = 0.0$–0.084 (Maddox et al. 2021) and the average M_{HI} and $M_\star$ measurements by Chowdhury et al. (2020, 2021) from stacking of the 21 cm signal of galaxies at $z \sim 1$–1.3. We further show the measurements from Heintz et al. (2021) based on the $\beta_{[CII]}$ conversion factor of galaxies in the range $z \sim 2$–6 surveyed for [C II] emission from the samples by Zanella et al. (2018), Capak et al. (2015) and the ALPINE-[C II] survey (Béthermin et al. 2020; Faisst et al. 2020; Le Fèvre et al. 2020). The majority of galaxies at $z \gtrsim 2$ show $M_{HI} > M_\star$ at all stellar masses. Galaxies at $z \lesssim 1$ mostly contain $M_{HI} \lesssim M_\star$ at large stellar masses ($M_\star \gtrsim 10^9 M_\odot$) but show increasing $M_{HI}/M_\star$ ratios at lower stellar masses.

The elevated H I gas mass fractions $M_{HI}/M_\star$ observed in the high-redshift galaxy samples are consistent with a gradual increase as a function of redshift, as illustrated in Figure 2. In this figure, we compare our measurements to the same local and high-redshift galaxy samples as compiled for Figure 1 and described above, relying on a combination of M_{HI} inferred via direct 21 cm observations and the $\beta_{[CII]}$ conversion. We find that the H I gas mass excess increases as a function of redshift, following approximately $M_{HI}/M_\star = 0.2 \times (1 + z)^{1.6}$, anchored to the median value inferred for the xGASS galaxy sample at $z = 0$. This relation is found to closely follow the redshift

evolution of the specific SFR (sSFR) recently measured by Topping et al. (2022).

To make a crude prediction for the average fraction of H I in the ISM out of the total baryonic matter content by mass (i.e., $M_{bar,tot} = M_{HI} + M_{H_2} + M_{\star}$) in these galaxies, we adopt an average [C II]-to-H_2 ratio of $\alpha_{[CII]} = 18$ (Vizgan et al. 2022). This yields a dominant H I component, with $M_{HI}/M_{bar,tot} = 60\%$. If we instead assume $\alpha_{[CII]} = 30$ (Zanella et al. 2018), we find a slightly lower, but still dominant, H I fraction of $M_{HI}/M_{bar,tot} = 55\%$. This suggests that H I dominates the baryonic matter content of galaxies in the epoch of reionization at $z \approx 7$. We further note that the predicted total gas masses $M_{gas} = M_{HI} + M_{H_2}$ of these high-z galaxies follow a relation on global scales similar to the local Kennicutt–Schmidt law (Kennicutt 1998) of surface densities $(SFR/M_{\odot} \, yr^{-1}) \propto (M_{gas}/M_{\odot})^n$ with $n = 1.2$–1.4, potentially hinting at the universality of this law even at $z \approx 7$.

4. The Cosmic H I Gas Mass Density in Galaxies at $z \approx 7$

We now consider the volume-averaged H I gas mass density (ρ_{HI}) in galaxies, related to the cosmological H I density Ω_{HI} via $\rho_{HI} = \Omega_{HI} \times \rho_c$, where ρ_c is the critical density of the universe[16]. This quantity has been constrained through various different approaches: at $z \sim 0$, extensive galaxy surveys of the 21 cm H I line emission have been used to infer the H I mass function, providing an estimate of ρ_{HI} (e.g., Zwaan et al. 2005; Braun 2012; Jones et al. 2018).

At intermediate redshifts ($z \sim 0.4$–1), ρ_{HI} can be constrained by stacking the 21 cm signal from a large ensemble of galaxies (e.g., Lah et al. 2007; Kanekar et al. 2016; Chowdhury et al. 2020) or via observations of the 21 cm feature in absorption toward radio-bright continuum sources (e.g., Grasha et al. 2020; Allison et al. 2022). At $z \gtrsim 2$ and up to $z \approx 5$, the H I gas mass density has primarily been constrained via the Lyα feature from intervening absorbers toward bright background quasars (see Péroux & Howk 2020, and references therein). These measurements, however, only constrain the fraction of H I gas in DLAs, $\rho_{HI, \, DLA}$, which may not be representative of the H I gas associated with star formation in galaxies at high redshifts, even though these systems contain the bulk (>85%) of the H I at all redshifts (Zwaan et al. 2005; O'Meara et al. 2007; Noterdaeme et al. 2012). We will address this point further below.

Following Heintz et al. (2021), we determine ρ_{HI} based on the [C II] 158 μm luminosity density, $\mathcal{L}_{[CII]}$, at $z \approx 7$. This approach follows a similar methodology to previous works that infer the cosmic H_2 gas mass density $\rho_{H_2}(z)$ based on the CO luminosity density (e.g., Walter et al. 2014; Decarli et al. 2019; Riechers et al. 2019). We adopt the [C II] 158 μm luminosity function (LF) parameters derived by P. Oesch et al. (2022, in preparation). based on the REBELS data to estimate the luminosity density as $\mathcal{L}_{[CII]} = \int_{L_{[CII]}}^{\infty} L_{[CII]} \phi(L_{[CII]}) dL_{[CII]}$. The [C II] 158 μm LF parameters considered in this work were determined by converting the UV LF to a [C II] LF. As prior, we use the UV LF from Bouwens et al. (2021) and the empirical L_{UV}–$L_{[CII]}$ relation (including an intrinsic dispersion), derived for galaxies at the same redshift. For more details, see P. Oesch et al. (2022, in preparation). We integrate over the full [C II] LF down to $\log(L_{[CII]}/L_{\odot}) = 7.5$, representing approximately the

REBELS detection limit (Bouwens et al. 2022; S. Schouws et al. 2022, in preparation). This yields a [C II] luminosity density of $\log(\mathcal{L}_{[CII]}/L_{\odot} \, Mpc^{-3}) = 4.85^{+0.25}_{-0.20}$ at $z \approx 7$. To infer ρ_{HI}, we assume an average gas-phase metallicity of $12 + \log(O/H) = 8.1$ $(\log(Z/Z_{\odot}) = -0.6)$ (Jones et al. 2020), to determine the average [C II]-to-H I conversion factor $\log \beta_{[CII]} = 2.00 \pm 0.13$ at this epoch. This yields a H I gas mass density of $\rho_{HI} = 7.1^{+6.4}_{-3.0} \times 10^6 \, M_{\odot} \, Mpc^{-3}$ in galaxies at $z \approx 7$, also shown in Figure 3.

To be consistent with this work, we rederive the value of $\mathcal{L}_{[CII]}$, and consequently ρ_{HI}, estimated by Heintz et al. (2021) at $z \approx 5$. This is based on the recent work by P. Oesch et al. (2022, in preparation), who find that adopting a similar L_{UV}–$L_{[CII]}$ relation as a prior to convert the $z \sim 5$ UV LF to a [C II] 158 μm LF yields results that are in good agreement with the stepwise [C II] LF points from Yan et al. (2020) measured from the ALPINE target sample. However, this [C II] LF lies significantly below the estimate obtained from the "serendipitous" $z \sim 5$ sources detected in the ALPINE survey as well as from estimates derived via the CO LF, which predict a vast excess of sources with $\log(L_{[CII]}/L_{\odot}) > 9$ compared to the ALPINE target sample (see Yan et al. 2020; Loiacono et al. 2021). This greatly affects the derivation of $\mathcal{L}_{[CII]}$, and thus also ρ_{HI}, which we find to be a factor of $\approx$10 lower than the previous estimate (at 3σ significance; Heintz et al. 2021). To be consistent with the REBELS LF, we chose to adopt the stepwise [C II] LF points derived for the ALPINE target sample by Yan et al. (2020), including the UV LF as a prior to better represent the underlying intrinsic galaxy population. For a more detailed discussion, see P. Oesch et al. (2022, in preparation). With this updated [C II]–158 μm LF, we estimate $\log(\mathcal{L}_{[CII]}/L_{\odot} \, Mpc^{-3}) = 5.37^{+0.19}_{-0.16}$ at $z \approx 5$, from which we now infer $\rho_{HI} = 1.6^{+1.1}_{-0.6} \times 10^7 \, M_{\odot} \, Mpc^{-3}$ as also shown in Figure 3. Overall, we find that ρ_{HI} increases by a factor of $\approx$10 from $z \approx 7$ to $z = 2$, to then turn over and decrease at later cosmic times, reaching $\rho_{HI} = 5 \times 10^7 \, M_{\odot} \, Mpc^{-3}$ at $z = 0$ (Péroux & Howk 2020; Walter et al. 2020).

In Figure 3 we compare our measurements of $\rho_{HI}(z)$ to other high-redshift estimates: $z \sim 0$–2 DLA measurements (Neeleman et al. 2016; Shull et al. 2017), combined 21 cm H I emission signal from star-forming galaxies at $z \approx 1$ (Chowdhury et al. 2020), results from a survey of 21 cm H I absorption systems at $z = 0$–2.74 (Grasha et al. 2020), and the recent compilation of $z \sim 2$–5 DLA measurements (see Péroux & Howk 2020; Walter et al. 2020, and references therein). We correct the values by 20% to account for the fraction of H I contained in sub-DLAs and Lyman-limit systems (e.g., Zafar et al. 2013) but do not include the contribution of helium as we are only interested in the amount of hydrogen in the form of H I.

Additionally, we compare our results to evolutionary trends of $\rho_{HI}(z)$, considering both the empirically determined $\rho_{HI,DLA}(z) = (5.8 \pm 0.3) \times 10^7 \times (1 + z)^{0.57 \pm 0.04}$ from the available DLA measurements (Péroux & Howk 2020), the global $\rho_{HI}(z)$ predicted by hydrodynamical simulations using various prescriptions for the inherent UV background (Maio et al. 2022), and the predictions for the evolution of the H I gas *in* galaxies from the "sub-res models" of the L-Galaxies simulations (Yates et al. 2021). The simulations by Maio et al. (2022) mainly track the amount of the cosmic gas mass density in neutral, atomic form, showing significant decreases at $z \approx 6$–8 from the initial state due to the reionization phase

---

[16] ρ_c is determined to be $\rho_c = 1.26 \times 10^{11} \, M_{\odot} \, Mpc^{-3}$ in the adopted ΛCDM cosmological paradigm (Planck Collaboration et al. 2020).
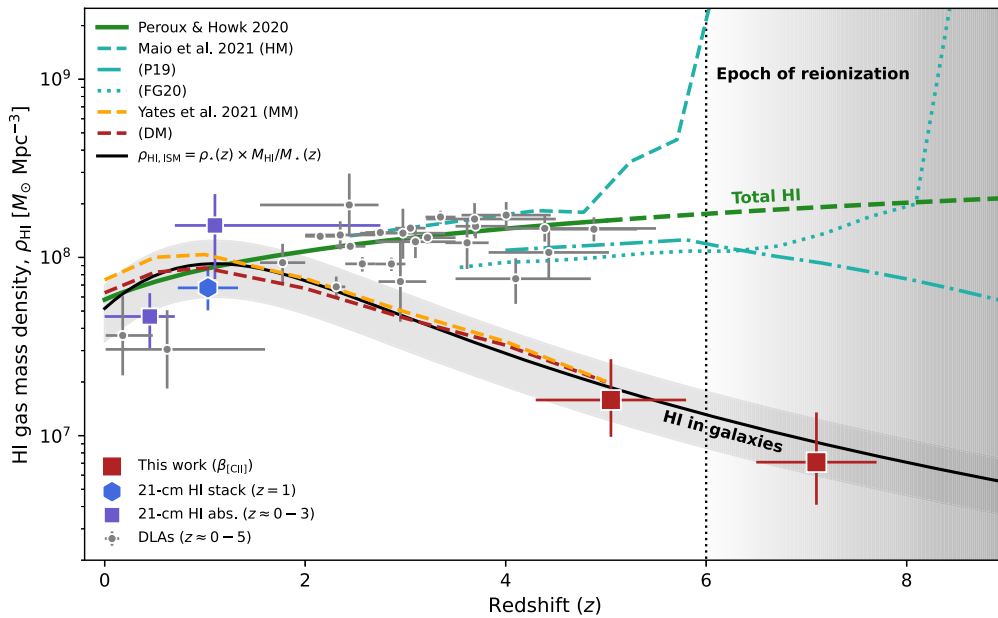
Figure 3. Redshift evolution of the cosmic H I gas mass density in galaxies, $\rho_{\rm HI}$. Measurements for this work (red squares) are based on the estimated [C II] luminosity densities at $z \sim 5$ and $z \sim 7$, converted to $\rho_{\rm HI}$. These results are largely dependent on the exact [C II] LF and may include significant systematic biases (see text). The blue hexagon shows the average measurement of galaxies at $z \sim 1$ from stacking of the 21 cm H I signal (Chowdhury et al. 2020) and purple squares show the results from a survey of intervening 21 cm H I absorption systems covering $0 < z < 0.69$ and $0.69 < z < 2.74$ (Grasha et al. 2020). The DLA measurements compiled by Walter et al. (2020) are shown by the gray dots, corrected by 20% to account for the contribution to H I from sub-DLAs and Lyman-limit systems. The green curve shows the best-fit evolution of $\rho_{\rm HI,DLA}(z)$ by Péroux & Howk (2020) based on DLA measurements and extrapolated beyond $z \gtrsim 5$ (shown as the dashed curve). The cyan curves show the $\rho_{\rm HI,tot}(z)$ predicted by hydrodynamical simulations using various prescriptions (HM, P19, and FG20; see Maio et al. 2022 and the main text). The orange and red dashed curves show the predictions for the evolution of H I inside galaxies from the default and modified model (DM, MM) of the L-Galaxies simulations by Yates et al. (2021). The black solid line shows the combined redshift evolution of the stellar-mass density $\rho_\star(z)$ determined by Walter et al. (2020) and the H I gas excess $M_{\rm HI}/M_\star$ derived in this work (see Section 3 and Figure 2), with the gray-shaded region marking the $\approx 35\%$ uncertainty on this evolutionary curve. The approximate end of the epoch of reionization is marked at $z \sim 6$.

transition. The L-Galaxies simulations described by Yates et al. (2021) on the other hand are by construction designed to only model the neutral gas inside galaxies. We further make a prediction for $\rho_{\rm HI,ISM}(z)$ in galaxies by combining the redshift evolution of the stellar-mass density $\rho_\star(z)$ from Walter et al. (2020, but here converted to a Chabrier IMF[17]) and the H I gas mass excess $M_{\rm HI}/M_\star \propto (1+z)^{1.6 \pm 0.2}$ derived in Section 3, as

$$\rho_{\rm HI,ISM}(z) = \rho_\star(z) \times M_{\rm HI}/M_\star(z) . \tag{3}$$

Propagating the uncertainties on the functions for $\rho_\star(z)$ and $M_{\rm HI}/M_\star(z)$ yields a relative uncertainty of $\approx 35\%$ on $\rho_{\rm HI,ISM}(z)$. We find that the evolution of $\rho_{\rm HI}(z)$ predicted from the simulations and DLA measurements shows a significant excess over the inferred values of $\rho_{\rm HI}$ from the [C II]-to-H I relation at $z \gtrsim 5$ from this work. We observe, however, a striking match between our measurements and the evolutionary trend predicted for $\rho_{\rm HI,ISM}(z)$ from Equation (3) and the L-Galaxies simulations by Yates et al. (2021). While both our measurements of $\rho_{\rm HI}$ and the function described by Equation (3) rely on the [C II]-to-H I conversion factor, we emphasize that one approach adopts the independently derived [C II]-158 μm LF, whereas the other is inferred from literature measurements of $\rho_\star(z)$ and the average redshift evolution of the H I gas mass excess. This discrepancy indicates that the majority of the H I gas probed by DLAs at $z \gtrsim 2$ is not associated with the star-forming regions of galaxies at this epoch.

We here propose a physical interpretation of this apparent discrepancy between $\rho_{\rm HI}$ measured from DLAs and via $\beta_{\rm [CII]}$. We argue that the former represents the total cosmic H I gas mass density, as expected given the random quasar sight lines through galaxies and the correction for the amount of H I in sub-DLAs and Lyman-limit systems, where the latter reflects the amount of H I contained in the neutral, star-forming ISM of galaxies. In this scenario, the evolutionary trend of $\rho_{\rm HI,ISM}(z)$ described by Equation (3) represents the buildup and accumulation of H I in galaxies, acting as the fundamental gas reservoir from which molecular gas and stars can be formed. On the other hand, the large excess of H I gas measured by quasar absorption-line systems at $z \gtrsim 3$ hints that the bulk of H I is located in the halos of galaxies at these redshifts and thus not directly associated with star formation (as also revealed by recent ALMA observations of quasar absorbers; Neeleman et al. 2019). This is also consistent with the recent simulations by Stern et al. (2021), in addition to Yates et al. (2021), who found that at least $\approx 65\%$ of the H I gas in the L-Galaxies, EAGLE, and TNG100 simulations have to be located in the outskirts of galaxies beyond $2\times$ the stellar half-mass radius at $z \gtrsim 3$. We quantify this relative ratio and thereby the buildup of H I in galaxies in Figure 4. Here, $\rho_{\rm HI,tot}$ is described by the empirical relation $\rho_{\rm HI,DLA}(z)$ from DLA sight lines (Péroux & Howk 2020), and $\rho_{\rm HI,ISM}$ is a measure of the H I associated with star formation in the neutral ISM probed by [C II] as described by Equation (3). We find that at $z \approx 3$ and beyond, the majority of H I ($\gtrsim 60\%$) is located in the halos or circumgalactic medium of galaxies. At $z \gtrsim 5$, only $\approx 10\%$ of H I confined in the ISM of galaxies. This simple model further predicts that by $z \approx 2$, the bulk of the extended H I gas

---

[17] Effectively we adopt $M_\star({\rm Chabrier}) = M_\star({\rm Salpeter})/1.5$.
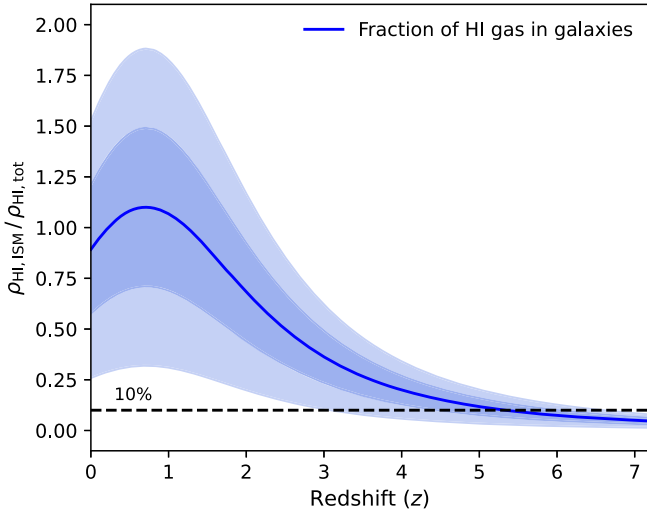
Figure 4. Fraction of H I in galaxies, $\rho_{HI,ISM}/\rho_{HI,tot}$, as a function of redshift. $\rho_{HI,ISM}$ measures the H I associated with star formation in the neutral ISM probed by [C II], whereas $\rho_{HI,tot}$ measures the total H I both in the ISM and the extended halos of galaxies probed by random quasar sight lines. Solid blue lines show the relative function and the dark- and light-shaded regions at the 1σ and 2σ confidence intervals. At $z \lesssim 2$, most ($\gtrsim 70\%$) of the H I gas has accreted into galaxies.

reservoirs will have accreted onto the galaxy ISM, exhausting the available circum- or intergalactic gas. We would like to caution though that this is only a first preliminary study on large cosmic time- and spatial scales, with potential biases related to sample statistics or different methods to probe the H I mass densities. We thus encourage complementary observations or simulations to further investigate and constrain this proposed scenario.

5. Summary and Outlook

We have here presented the first measurements of the neutral atomic hydrogen (H I) gas content of star-forming galaxies during the epoch of reionization. This work is based on the sample of galaxies at $z = 6.5$–7.8 surveyed for [C II] 158 μm emission as part of the REBELS survey (Bouwens et al. 2022). Combined with a recent calibration of the [C II]-to-H I conversion factor, $\beta_{[CII]} = M_{HI}/L_{[CII]}$, we inferred the H I gas masses of the individual galaxies in this survey based on the [C II] luminosities, $L_{[CII]}$. We found an average H I gas mass excess of $M_{HI}/M_\star \approx 10$, corresponding to an average H I gas mass fraction of $f_{HI} = M_{HI}/(M_\star + M_{HI}) \approx 90\%$. These results are consistent with an overall, gradual increase of $M_{HI}/M_\star$ and f_{HI} with redshift. Further, they provide the first evidence that H I is the dominant baryonic component by mass in galaxies from the epoch of reionization to $z \approx 2$.

We further used the $\beta_{[CII]}$ conversion factor to make predictions for the cosmic H I gas mass density in galaxies (ρ_{HI}) at $z \approx 7$ based on recent estimates of the [C II] 158 μm luminosity function at this epoch. We found that ρ_{HI} increases by a factor of ≈ 10 from $z \approx 7$ to $z \approx 2$, with $\rho_{HI} = 7.1^{+6.4}_{-3.0} \times 10^6 \, M_\odot \, \mathrm{Mpc}^{-3}$ at $z \approx 7$. We argued that this increase reflects the accretion and buildup of H I onto galaxies, associated with the star-forming ISM as traced by [C II]. Notably, this evolutionary trend shows a large deficit of H I when compared to measurements from DLA sight lines and predictions of the global H I gas content from hydrodynamical simulations at similar cosmic epochs. To explain this apparent discrepancy,

we proposed a scenario where the DLA sight lines mainly probe H I in the halos of galaxies at $z \gtrsim 2$, thereby not associated with the bulk of star formation. This indicates that the fraction and distribution of H I in halos and in the ISM of galaxies are markedly different at low and high redshifts.

These results emphasize the need to also take into account the neutral atomic gas phase, which may be the dominant baryonic component of high-z galaxies, instead of assuming that the molecular gas phase is the sole contributor to M_{gas} as done previously (e.g., Förster Schreiber & Wuyts 2020; Tacconi et al. 2020). Ignoring H I might affect dynamical studies, inferred gas depletion timescales, and the overall assembly history of gas in galaxies and stellar-mass buildup. Recently, Walter et al. (2020) demonstrated that the growth in stellar mass cannot be accounted for by the decrease in the cosmic H_2 gas in galaxies, requiring significant infall of additional pristine gas. Here we constrained this exact process, disentangling the amount of H I in and outside of galaxies through cosmic time. The H I gas in galaxies associated with the star-forming ISM acts as the transition state between the circumgalactic hot halo gas and the cool, molecular gas phase providing the fuel for star formation.

With the advent of the next-generation radio facilities such as the Square Kilometre Array (SKA), it will soon be possible to survey H I directly through the 21 cm transition from individual galaxies beyond what is currently achievable (Blyth et al. 2015). SKA pathfinder telescopes such as MeerKAT have already shown great promise in extending the redshift range for which the 21 cm H I emission can be detected in individual galaxies (Maddox et al. 2021). However, even with the SKA, it will still be challenging to detect H I directly from galaxies much beyond $z > 0.5$. Statistical approaches averaging the spectra of known galaxies (Chowdhury et al. 2020) or intensity mapping (Santos et al. 2015) might potentially alleviate this technical limitation but still only provide an average census of H I in galaxies at the surveyed redshifts. Using [C II] as a proxy for H I is therefore the current best alternative to probe the neutral atomic gas phase in galaxies beyond the local universe and out to the epoch of reionization.

Data availability statement

Source codes for the figures and tables presented in this article are available from the corresponding author upon reasonable request.

ORCID iDs

K. E. Heintz ⓘ https://orcid.org/0000-0002-9389-7413
P. A. Oesch ⓘ https://orcid.org/0000-0001-5851-6649
M. Aravena ⓘ https://orcid.org/0000-0002-6290-3198
R. J. Bouwens ⓘ https://orcid.org/0000-0002-4989-2471
P. Dayal ⓘ https://orcid.org/0000-0001-8460-1564
A. Ferrara ⓘ https://orcid.org/0000-0002-9400-7312
Y. Fudamoto ⓘ https://orcid.org/0000-0001-7440-8832
L. Graziani ⓘ https://orcid.org/0000-0002-9231-1505
H. Inami ⓘ https://orcid.org/0000-0003-4268-0393
L. Sommovigo ⓘ https://orcid.org/0000-0002-2906-2200
R. Smit ⓘ https://orcid.org/0000-0001-8034-7802
M. Stefanon ⓘ https://orcid.org/0000-0001-7768-5309
M. Topping ⓘ https://orcid.org/0000-0001-8426-1141
A. Pallottini ⓘ https://orcid.org/0000-0002-7129-5761
P. van der Werf ⓘ https://orcid.org/0000-0001-5434-5942

References

Allison, J. R., Sadler, E. M., Amaral, A. D., et al. 2022, PASA, 39, e010
Asplund, M., Grevesse, N., Sauval, A. J., & Scott, P. 2009, ARA&A, 47, 481
Bañados, E., Rauch, M., Decarli, R., et al. 2019, ApJ, 885, 59
Béthermin, M., Fudamoto, Y., Ginolfi, M., et al. 2020, A&A, 643, A2
Blyth, S., van der Hulst, T. M., Verheijen, M. A. W., et al. 2015, in Proc. of Advancing Astrophysics with the Square Kilometre Array (AASKA14) (Trieste: SISSA), 128
Bolatto, A. D., Wolfire, M., & Leroy, A. K. 2013, ARA&A, 51, 207
Bouwens, R. J., Oesch, P. A., Stefanon, M., et al. 2021, AJ, 162, 47
Bouwens, R. J., Smit, R., Schouws, S., et al. 2022, ApJ, 931, 160
Braun, R. 2012, ApJ, 749, 87
Capak, P. L., Carilli, C., Jones, G., et al. 2015, Natur, 522, 455
Carilli, C. L., & Walter, F. 2013, ARA&A, 51, 105
Catinella, B., Saintonge, A., Janowiecki, S., et al. 2018, MNRAS, 476, 875
Chabrier, G. 2003, PASP, 115, 763
Chowdhury, A., Kanekar, N., Chengalur, J. N., Sethi, S., & Dwarakanath, K. S. 2020, Natur, 586, 369
Chowdhury, A., Kanekar, N., Das, B., Dwarakanath, K. S., & Sethi, S. 2021, ApJL, 913, L24
Cormier, D., Madden, S. C., Lebouteiller, V., et al. 2015, A&A, 578, A53
Croxall, K. V., Smith, J. D., Pellegrini, E., et al. 2017, ApJ, 845, 96
Curti, M., Mannucci, F., Cresci, G., & Maiolino, R. 2020, MNRAS, 491, 944
Dayal, P., & Ferrara, A. 2018, PhR, 780, 1
Dayal, P., Ferrara, A., Sommovigo, L., et al. 2022, MNRAS, 512, 989
Decarli, R., Walter, F., Gónzalez-López, J., et al. 2019, ApJ, 882, 138
Endsley, R., Stark, D. P., Bouwens, R. J., et al. 2022, arXiv:2202.01219
Faisst, A. L., Schaerer, D., Lemaux, B. C., et al. 2020, ApJS, 247, 61

Fernández, X., Gim, H. B., van Gorkom, J. H., et al. 2016, ApJL, 824, L1
Ferrara, A., Sommovigo, L., Dayal, P., et al. 2022, MNRAS, 512, 58
Förster Schreiber, N. M., & Wuyts, S. 2020, ARA&A, 58, 661
Fudamoto, Y., Smit, R., Bowler, R. A. A., et al. 2022, arXiv:2206.01886
Grasha, K., Darling, J., Leroy, A. K., & Bolatto, A. D. 2020, MNRAS, 498, 883
Hashimoto, T., Inoue, A. K., Mawatari, K., et al. 2019, PASJ, 71, 71
Heintz, K. E., & Watson, D. 2020, ApJL, 889, L7
Heintz, K. E., Watson, D., Oesch, P. A., Narayanan, D., & Madden, S. C. 2021, ApJ, 922, 147
Hutter, A., Dayal, P., Yepes, G., et al. 2021, MNRAS, 503, 3698
Inami, H., Algera, H. S. B., Schouws, S., et al. 2022, MNRAS, Advance Access
Jones, M. G., Haynes, M. P., Giovanelli, R., & Moorman, C. 2018, MNRAS, 477, 2
Jones, T., Sanders, R., Roberts-Borsani, G., et al. 2020, ApJ, 903, 150
Kanekar, N., Sethi, S., & Dwarakanath, K. S. 2016, ApJL, 818, L28
Katz, H., Kimm, T., Sijacki, D., & Haehnelt, M. G. 2017, MNRAS, 468, 4831
Kennicutt, R. C. J. 1998, ARA&A, 36, 189
Lah, P., Chengalur, J. N., Briggs, F. H., et al. 2007, MNRAS, 376, 1357
Le Fèvre, O., Béthermin, M., Faisst, A., et al. 2020, A&A, 643, A1
Leja, J., Johnson, B. D., Conroy, C., van Dokkum, P. G., & Byler, N. 2017, ApJ, 837, 170
Leroy, A. K., Walter, F., Brinks, E., et al. 2008, AJ, 136, 2782
Loiacono, F., Decarli, R., Gruppioni, C., et al. 2021, A&A, 646, A76
Madden, S. C., Geis, N., Genzel, R., et al. 1993, ApJ, 407, 579
Madden, S. C., Poglitsch, A., Geis, N., Stacey, G. J., & Townes, C. H. 1997, ApJ, 483, 200
Madden, S. C., Rémy-Ruyer, A., Galametz, M., et al. 2013, PASP, 125, 600
Maddox, N., Frank, B. S., Ponomareva, A. A., et al. 2021, A&A, 646, A35
Magdis, G. E., Daddi, E., Béthermin, M., et al. 2012, ApJ, 760, 6
Maio, U., Péroux, C., & Ciardi, B. 2022, A&A, 657, A47
Matthee, J., Sobral, D., Boogaard, L. A., et al. 2019, ApJ, 881, 124
Meyer, R. A., Walter, F., Cicone, C., et al. 2022, ApJ, 927, 152
Neeleman, M., Kanekar, N., Prochaska, J. X., Rafelski, M. A., & Carilli, C. L. 2019, ApJL, 870, L19
Neeleman, M., Prochaska, J. X., Ribaudo, J., et al. 2016, ApJ, 818, 113
Noterdaeme, P., Petitjean, P., Carithers, W. C., et al. 2012, A&A, 547, L1
Novak, M., Bañados, E., Decarli, R., et al. 2019, ApJ, 881, 63
Olsen, K. P., Greve, T. R., Narayanan, D., et al. 2015, ApJ, 814, 76
O'Meara, J. M., Prochaska, J. X., Burles, S., et al. 2007, ApJ, 656, 666
Pallottini, A., Ferrara, A., Decataldo, D., et al. 2019, MNRAS, 487, 1689
Papadopoulos, P. P., Thi, W. F., & Viti, S. 2004, MNRAS, 351, 147
Péroux, C., & Howk, J. C. 2020, ARA&A, 58, 363
Péroux, C., McMahon, R. G., Storrie-Lombardi, L. J., & Irwin, M. J. 2003, MNRAS, 346, 1103
Pineda, J. L., Langer, W. D., & Goldsmith, P. F. 2014, A&A, 570, A121
Planck Collaboration, Aghanim, N., Akrami, Y., et al. 2020, A&A, 641, A6
Prochaska, J. X., & Wolfe, A. M. 2009, ApJ, 696, 1543
Ramos Padilla, A. F., Wang, L., van der Tak, F. F. S., & Trager, S. 2022, arXiv:2205.11955
Rémy-Ruyer, A., Madden, S. C., Galliano, F., et al. 2014, A&A, 563, A31
Riechers, D. A., Pavesi, R., Sharon, C. E., et al. 2019, ApJ, 872, 7
Sanders, R. L., Shapley, A. E., Jones, T., et al. 2021, ApJ, 914, 19
Santos, M., Bull, P., Alonso, D., et al. 2015, in Proc. of Advancing Astrophysics with the Square Kilometre Array (AASKA14) (Trieste: SISSA), 19
Schouws, S., Bouwens, R., Smit, R., et al. 2022, arXiv:2202.04080
Scoville, N., Lee, N., Vanden Bout, P., et al. 2017, ApJ, 837, 150
Shull, J. M., Danforth, C. W., Tilton, E. M., Moloney, J., & Stevens, M. L. 2017, ApJ, 849, 106
Smit, R., Bouwens, R. J., Carniani, S., et al. 2018, Natur, 553, 178
Sommovigo, L., Ferrara, A., Pallottini, A., et al. 2022, MNRAS, 513, 3122
Stern, J., Sternberg, A., Faucher-Giguère, C.-A., et al. 2021, MNRAS, 507, 2869
Tacconi, L. J., Genzel, R., Neri, R., et al. 2010, Natur, 463, 781
Tacconi, L. J., Genzel, R., Saintonge, A., et al. 2018, ApJ, 853, 179
Tacconi, L. J., Genzel, R., & Sternberg, A. 2020, ARA&A, 58, 157
Topping, M. W., Stark, D. P., Endsley, R., et al. 2022, arXiv:2203.07392
Ucci, G., Dayal, P., Hutter, A., et al. 2021, arXiv:2112.02115
Valentino, F., Magdis, G. E., Daddi, E., et al. 2018, ApJ, 869, 27
Vallini, L., Ferrara, A., Pallottini, A., & Gallerani, S. 2017, MNRAS, 467, 1300
Vizgan, D., Greve, T. R., Olsen, K. P., et al. 2022, ApJ, 929, 92
Walter, F., Brinks, E., de Blok, W. J. G., et al. 2008, AJ, 136, 2563

Walter, F., Carilli, C., Neeleman, M., et al. 2020, ApJ, 902, 111
Walter, F., Decarli, R., Sargent, M., et al. 2014, ApJ, 782, 79
Walter, F., Weiß, A., Downes, D., Decarli, R., & Henkel, C. 2011, ApJ, 730, 18
Yan, L., Sajina, A., Loiacono, F., et al. 2020, ApJ, 905, 147

Yates, R. M., Péroux, C., & Nelson, D. 2021, MNRAS, 508, 3535
Zafar, T., Péroux, C., Popping, A., et al. 2013, A&A, 556, A141
Zanella, A., Daddi, E., Magdis, G., et al. 2018, MNRAS, 481, 1976
Zwaan, M. A., Meyer, M. J., Staveley-Smith, L., & Webster, R. L. 2005, MNRAS, 359, L30